Applied Catalysis B: Environmental 338 (2023) 123080

Contents lists available at ScienceDirect

Applied Catalysis B: Environmental

journal homepage: www.elsevier.com/locate/apcatb

Iodide-mediated selective photocatalytic treatment of phenolic pollutants

Liangpang Xu [a], Po Keung Wong [b], Zhifeng Jiang [c,*], Jimmy C. Yu [a,*]

[a] Department of Chemistry, The Chinese University of Hong Kong, Shatin, New Territories 999077, Hong Kong, China
[b] School of Life Sciences, The Chinese University of Hong Kong, Shatin, New Territories 999077, Hong Kong, China
[c] Institute for Energy Research, Jiangsu University, Zhenjiang 212013, China

ARTICLE INFO

Keywords:
Photocatalysis
Iodide oxidation
Reactive iodine species
Selective oxidation
Phenolic pollutants

ABSTRACT

Photocatalysis is a promising approach for environmental remediation. However, the intensively studied •OH and h^+-based oxidation processes often miss the target pollutants due to their poor selectivity. The potential formation of toxic degradation byproducts from the oxidation of matrix species is a real concern in photocatalytic treatment. Here, we describe an innovative application of iodide-based photocatalytic process towards efficient degradation of phenolic pollutants even in complex water matrixes. Due to the presence of iodide, the degradation rate of our target pollutant, bisphenol A (BPA), was enhanced by 29 times on g-C_3N_4, and as much as 130 times on CdS. With evolved reactive iodine species (RIS) as oxidants, the iodide-based photocatalysis could selectively oxidize phenolic pollutants, thus, avoiding the inhibition by ubiquitous anions and organics in wastewater. Quenching experiments and measurements of RIS demonstrated that the diiodide ($•I_2$) was the dominant oxidant for degradation of phenolic pollutants, while iodine atom (•I) and triiodide (I_3) play minor roles. This work sheds light on the practical application of iodide-based photocatalysis for water treatment.

1. Introduction

Phenolic compounds are one of the ubiquitous organic pollutants in the effluents (up to thousands of mg L^{-1}) from a variety of industrials, such as petrochemical, petroleum refinery, coke-to-chemicals, leather, printing and dyeing [1,2]. Due to the acute and chronic toxicity to humans and other organisms even at low concentrations (several mg L^{-1}), phenolics have been designated as the priority pollutants by the US Environmental Protection Agency (EPA) [1]. To remove the organic pollutants from effluents, a series of methods have been developed, such as photocatalysis [3], advanced oxidation processes (AOPs) [4,5], biodegradation [6], etc. As a green and sustainable technology, the solar-driven photocatalysis has been usually considered a promising approach among them [7,8]. A large amount of semiconductive materials have been studied for environmental photocatalysis [7,9], and g-C_3N_4 and TiO_2 are two of the most classic photocatalysts [10,11].

Nevertheless, conventional photocatalytic approaches are not optimized for efficient treatment of organic pollutants in complex water matrixes. Typically, photocatalytic degradation relies on generation of reactive oxidizing species, mainly hydroxyl radicals (•OH) and holes (h^+) (Fig. 1) [9,12]. However, due to the rapid recombination of photo-induced e^--h^+ pairs [13,14], poor h^+ is available for oxidation of pollutants, so does the •OH derived from water oxidation by h^+ [15], or oxygen reduction by e^- [16]. As thus, few oxidative species are available for pollutant degradation. Besides, selective treatment of target organic pollutants in complex matrixes (e.g. high salinity water) remains a non-negligible issue for environmental photocatalysis [17]. Due to the strong oxidizability (e.g. ~2.7 V vs NHE for h^+ of TiO_2 and •OH) [18], the h^+ and •OH are able to oxidize various anions (e.g. Cl^-, CO_3^{2-}) and organics (e.g. small organic acids) commonly presented in wastewater and nature waters [19,20], without specific selectivity towards organic pollutants. Such •OH/h^+-based non-selective oxidation processes could strongly restrain photocatalytic degradation. Firstly, due to the scavenging of •OH/h^+ by ubiquitous anions and organics [21–23], the degradation efficiency of target organic pollutants would suffer from significant inhibition. Furthermore, the oxidation of non-target compounds may produce intermediates with more negative environmental impacts [17]. For example, the reaction between •OH and salicylic acid would produce intermediates with dramatically increased toxicity [24]. Therefore, photocatalytic process simultaneously owns high efficiency and selectivity towards specific pollutants would be a more promising approach for practical wastewater treatment.

Iodide-mediated photocatalysis could be a strategy of killing two birds with one stone for efficient and selective treatment of organic

* Corresponding authors.
E-mail addresses: jiangzf@ujs.edu.cn (Z. Jiang), jimyu@cuhk.edu.hk (J.C. Yu).

https://doi.org/10.1016/j.apcatb.2023.123080
Received 8 April 2023; Received in revised form 16 June 2023; Accepted 6 July 2023
Available online 8 July 2023
0926-3373/© 2023 Elsevier B.V. All rights reserved.

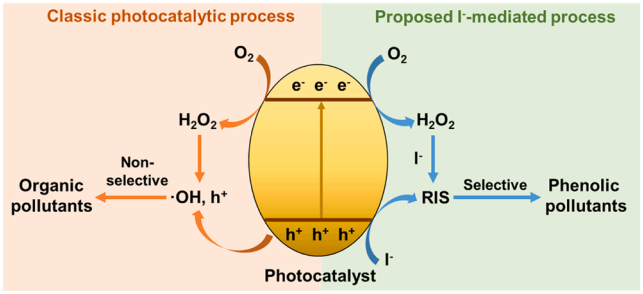

Fig. 1. Comparing the classic and proposed I-mediated photocatalytic processes for treatment of organic pollutants.

pollutants. Given a moderate redox potential (E^0(•I/I$^-$) = 1.33 V vs NHE), the iodide (I$^-$) is thermodynamically favorable to be oxidized by reactive species (e.g. h^+ and H_2O_2) generated in photocatalytic process [25]. The produced reactive iodine species (RIS, such as •I, •I_2^-, I_2, and HIO) as effective oxidants have attracted increasing attention for water treatment [26–28]. The I$^-$-mediated photocatalysis has great potential to simultaneously address the issues of efficiency and selectivity in photocatalytic pollutant degradation. Once photo-generated h^+ is consumed for I$^-$ oxidation, more e^- will be available for reduction of dissolved oxygen to generate H_2O_2 [29], which can also oxidize I$^-$ (Fig. 1) [28]. As such, RIS can be efficiently produced to rapidly degrade organic pollutants. Importantly, the RIS exhibits unique selectivity towards phenolic pollutants [27]. The RIS own a weaker oxidation ability (e.g. E^0(•I/I$^-$) = 1.33 V, E^0(•I_2^-/2I$^-$) = 1.03 V) compared with h^+ and •OH [30], and therefore are less likely to be consumed by common substances in water. The RIS mainly oxidize pollutants via one-electron transfer [31], which is different from the pathway of H-abstraction and addition for •OH. Furthermore, RIS are less reactive towards carboxylic acids and alcohols [32], which are the common degradation products of organic pollutants. To date, though there have been studies on the I$^-$ chemistry in dye-sensitized solar cells and TiO_2-based photocatalysis [25,33], the significant application of I$^-$-based photocatalysis in environmental treatment and the underlying mechanism are rarely investigated.

In this work, we reported an innovative I$^-$-mediated photocatalytic process for efficient and selective degradation of phenolic pollutants. Systematical study for the degradation of organic pollutants by the I$^-$-involved photocatalytic system was conducted. Significantly enhanced removal of bisphenol A (BPA) was achieved with the degradation rate increased by as much as 20–130 times due to the presence of I$^-$. Degradation of a series of representative phenolic compounds (bisphenol A, 2,4-dichlorophenol, 2,2′-biphenol, and p-cresol) and nonphenolic compounds (rhodamine B and ibuprofen) with diverse structures were studied to evaluate the capability and selectivity of the I$^-$-involved photocatalytic system. Measurements of RIS indicate a mechanism involving •I_2^- as the major, and I_3^- and •I as minor oxidants, respectively. Finally, the pathway for generation of RIS in photocatalytic process was also demonstrated.

2. Experimental section

2.1. Chemicals and materials

Potassium iodide (99%) and melamine (99%) were purchased from Energy Chemical Co. LTD (Shanghai, China). Bisphenol A, p-cresol, 2,2′-biphenol, and 2,4-dichlorophenol were purchased from J&K Scientific Ltd (Beijing, China). Ibuprofen and Rhodamine B were purchased from Yihe Biotech Co., Ltd. (Shanghai, China). Potassium chloride, potassium sulfate, dipotassium phosphate, and potassium bicarbonate were purchased from Scharlau (Barcelona, Spain). Ultrapure water (18.2 MΩ cm) was supplied by an ELGA Labwater system (PURELAB Ultra, ELGA LabWater Global Operations, UK). All reagents were of analytical grade and used without further purification.

The K-doped g-C_3N_4 (KCN) was synthesized by using melamine (1.5 g) and potassium chloride (0.75 g) as precursors. Firstly, the precursors were completely grinded, and then put into a ceramic crucible (10 mL) for heating. After thermal treatment at 550 °C for 4 h with a temperature rise rate of 5 °C min^{-1}, the product was washed with deionized water for several times, and dried in an oven at 60 °C for 48 h. Pristine g-C_3N_4 (CN) was prepared similarly, but without involving potassium chloride in the precursor. Cl-doped g-C_3N_4 (Cl-CN) was prepared the same as KCN, except for using NaCl to replace KCl. Bismuth chloride (BiOCl) was prepared as described in our previous studies [34]. Commercial titanium dioxide (TiO_2) (TCI, Japan) and cadmium sulfide (CdS) (Farco Chemical, China) was directly used. The characterization of catalysts was included in Supporting Information (Text S1).

2.2. Experimental procedures

The catalyst (25 mg) was suspended in ultrapure water (50 mL) by ultrasonication (20 min). Then, KI and pollutants were added to the suspension, followed by continuous stir in the dark (30 min) to reach sorption-desorption equilibrium. Afterwards, the suspension was transferred into a jacketed beaker (100 mL), which was equipped with a water-circulating system to keep a steady-state reaction temperature (20 °C). A 300 W xenon lamp (PLS-SXE300, Beijing Perfectlight Technology Co., Ltd., China) was used in all experiments involving irradiation, and a 420 nm cutoff filter was further equipped for visible-light irradiation. During the irradiation, the suspension was sampled at designed time intervals, and then filtered (0.22 μm) prior to final concentration analysis.

2.3. Analysis method

The concentration of all phenolic pollutants was determined using an Agilent 1260 high-performance liquid chromatography (HPLC), which is equipped with a 4.6 × 150 mm^2 SB-C18 separation column. The mobile phase includes water and methanol in different volume ratios, 65%:35% for bisphenol A, 45%:55% for 2,2′-biphenol and p-cresol, and 37%:63% for 2, 4-dichlorophenol. The mobile phase for ibuprofen is 25% phosphoric acid (0.1 vol%):75% methanol. A UV detector was used for most pollutants (220 nm for ibuprofen, and 280 nm for the others), and a fluorescence detector was used for p-cresol (E_x: 284 nm, E_m: 310 nm). Rhodamine B was analyzed using a UV–vis spectrophotometer (Cary 100, Agilent).

2.4. Measurement of reactive species

The photocatalytic generation of RIS was monitored by a spectrometric method. The generated •I though oxidation of I$^-$ could further react with I$^-$ to form I_3^-, which own classic absorbance at the wavelength of 350 nm with a molar extinction coefficient of 26400 M^{-1} cm^{-1} [35]. After determining the production of I_3^-, the I_2 yield could be determined based on the molar extinction coefficients of I_2 and I_3^- at 460 nm (746 and 975 M^{-1} cm^{-1}, respectively) [35]. To determine the pathway for oxidation of I$^-$, the role of h^+ and H_2O_2 were evaluated by quenching experiments together with measurement of H_2O_2 generation. A classic I_3^- method was used to analyze the concentration of H_2O_2: the sample was mixed with phthalic acid (0.1 M) and potassium iodide (0.4 M) in a volume ratio of 1:1:1, and then leave the solution in dark for 30-minutes color development. The absorbance of samples were measured using a UV-vis spectrophotometer.

3. Results and discussion

3.1. Characterization of catalysts

Similar to CN, the KCN displays a layer structure stacked by nanosheets as illustrated in the scanning electron microscopy (SEM) and transmission electron microscopy (TEM) images (Fig. S1). In the XRD patterns, typical peaks of CN at 13.2° (100) and 27.4° (002) are observed for KCN, and the TiO_2 is anatase phase (Fig. S2). According to the Fourier-transform infrared spectroscopy (FT-IR) spectra (Fig. S3), the KCN exhibits classic heterocyclic C-N structure of g-C_3N_4, except for the more significant signals of cyano groups [16]. The energy dispersive X-ray spectrometry (EDS) mapping images demonstrate the presence of K in KCN (7.4% in atomic ratio determined by X-ray photoelectron spectroscopy, XPS), and the uniform distributions of all atoms (i.e. C, N, K, O, and Cl) in KCN (Fig. S4). Doping of K has been widely accepted as an effective approach to improve the light absorption and separation efficiency of charge carriers [36,37]. The light absorption edge of KCN is approximately 487 nm (Fig. S5), corresponding to a bandgap of 2.56 eV, 0.14 eV narrower than that of CN (2.7 eV). The band structure of KCN was calculated according to the Mott-Schottky plot and valence band XPS spectrum (Fig. S5b-c), and the result is summarized in Fig. S5d. It could be found that oxygen reduction and iodide oxidation are thermodynamically favorable for KCN. The BET surface areas of KCN and TiO_2 are 21.38 and 22.73 $m^2\ g^{-1}$, respectively.

3.2. I⁻-enhanced photocatalytic degradation

Although g-C_3N_4-based photocatalysis has been extensively studied for treatment of pollutants, the performance of classic photocatalytic system of KCN, however, is still rather limited in terms of degradation of bisphenol A (BPA) (Fig. 2a). The degradation rate of BPA is merely 0.15 h^{-1}, which means that it needs more than 30.7 h to reach a removal efficiency > 99%. Such a low activity could be attributed to the inefficient generation of reactive oxidizing species (e.g. h^+ and •OH) due to the fast recombination of photo-generated e^--h^+ pairs of KCN [38], which is commonly observed in g-C_3N_4-based photocatalysis [39]. Nevertheless, by introducing I^- into the photocatalytic system, the degradation of BPA was significantly enhanced (Fig. 2a). The BPA degradation on KCN is obviously faster than that on both pristine g-C_3N_4 (CN) and Cl-doped g-C_3N_4 (Cl-CN) (Fig. S6), suggesting the key role of K-doping on improving the activity of KCN. The BPA degradation is well fitted by the pseudo-first-order kinetic model ($R^2 > 0.90$), and the corresponding rate constants (k_{BPA}) were calculated and summarized in Table 1. Compared with the system without I^-, the k_{BPA} increased by 29 times with the presence of 40 mM I^-, and the estimated half-lives ($t_{1/2}$) decreased from 4.56 to 0.15 h (Table 1). However, other halogen ions (i.e. Cl^- and Br^-) exhibit negligible enhancement on BPA degradation (Fig. S7). This is because the oxidation potential of Cl^- and Br^- are close to that of water, and thus there is severe competition between Cl^-/Br^- and water for photo-generated h^+ of KCN [40], while the I^- oxidation (0.54 V vs RHE) is thermodynamically much more favorable (Fig. S5d). In combination with the potential I^- oxidation by H_2O_2 generated from O_2 reduction by photo-generated e^- [28], the I^- oxidation to form reactive species would more favorable compared with Cl^- and Br^-. These results demonstrate the great potential of the I^--based photocatalytic system for advanced treatment of organic pollutants.

TiO_2 is another widely used photocatalyst for environmental treatment. Hence, the I^--mediated photocatalytic degradation of BPA on TiO_2 was also tested, and the results were shown in Fig. 2b. Similarly, the BPA degradation rate is greatly enhanced by 20 times with the presence of increasing concentration of I^- until 40 mM, while the $t_{1/2}$ of BPA was

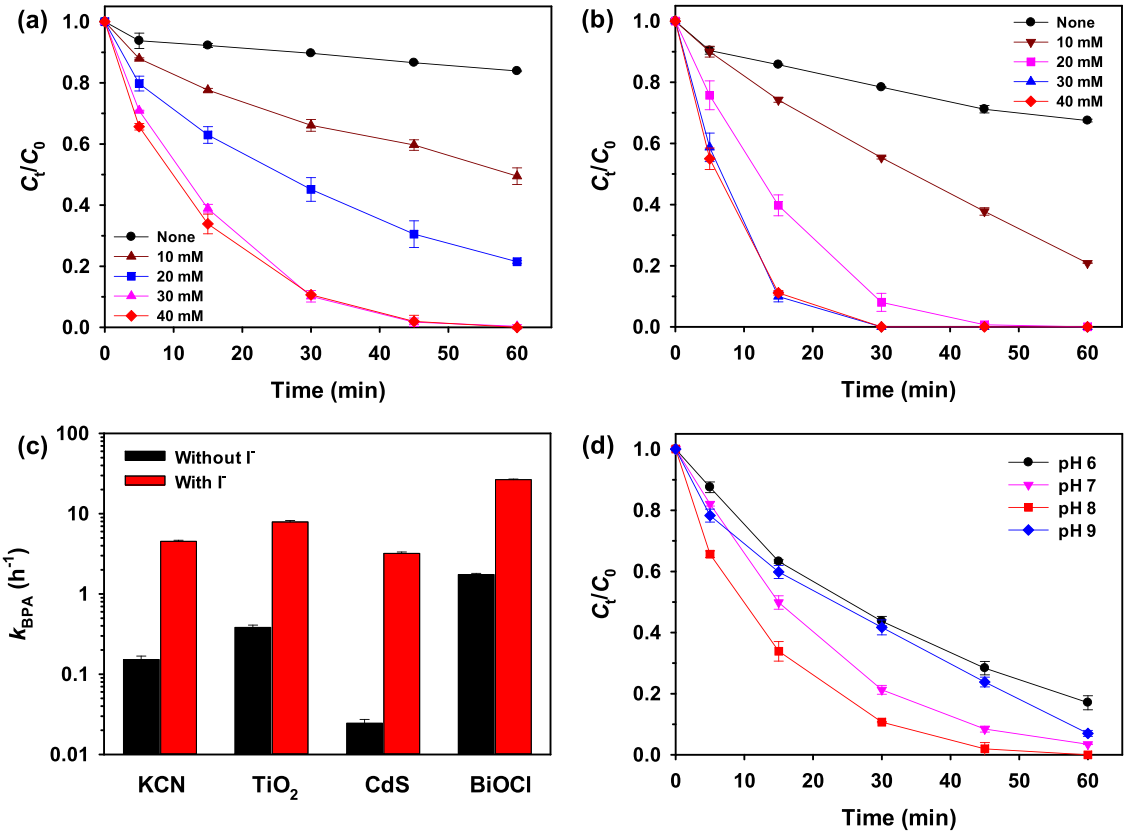

Fig. 2. Photocatalytic degradation of bisphenol A (BPA) (100 μM) in the presence of different concentrations of I^- at pH 8 over (a) KCN, and (b) TiO_2. (c) BPA degradation rates for various photocatalysts (CdS, KCN, BiOCl, and TiO_2) in the presence/absence of I^- (40 mM). (d) BPA degradation on KCN in the presence of I^- (40 mM) at different pH. Error bars represent standard variations from duplicate measurements.

Table 1
Fitting parameters for BPA degradation by photocatalytic I–based system with pseudo-first-order model.[a].

Reaction condition	k_{BPA} (h^{-1})[b]	R^2	$t_{1/2}$ (h)[c]
KCN	0.15 ± 0.02	0.90	4.56
KCN + I^- (10 mM)	0.68 ± 0.04	0.97	1.02
KCN + I^- (20 mM)	1.55 ± 0.08	0.98	0.45
KCN + I^- (30 mM)	4.14 ± 0.15	1.00	0.17
KCN + I^- (40 mM)	4.53 ± 0.15	1.00	0.15
TiO_2 + I^-	0.38 ± 0.03	0.96	1.80
TiO_2 + I^- (10 mM)	1.35 ± 0.06	0.99	0.51
TiO_2 + I^- (20 mM)	4.13 ± 0.26	0.99	0.17
TiO_2 + I^- (30 mM)	7.64 ± 0.49	0.99	0.09
TiO_2 + I^- (40 mM)	7.91 ± 0.32	1.00	0.09
CdS	0.02 ± 0.00	0.90	28.20
BiOCl	3.22 ± 0.12	1.00	0.22
CdS + I^- (40 mM)	1.74 ± 0.06	0.99	0.40
BiOCl + I^- (40 mM)	26.56 ± 0.46	1.00	0.03

[a] Reaction conditions: 100 μM BPA, 0.5 g/L catalyst, pH 8, visible-light irradiation at 20 °C.
[b] Apparent pseudo-first-order rate constants determined as the slope of linear regression with a 95% confidence interval.
[c] Half-lives calculated by the equation: $t_{1/2} = \ln 2/k_{BPA}$.

shortened from 1.8 to 0.09 h (Table 1). Besides KCN and TiO_2, the effect of I^- on BPA degradation was examined for other well-studied photocatalysts, including CdS and BiOCl. As shown in Fig. 2c, the I^--induced promoting effect for BPA degradation was also observed on CdS and BiOCl. With 40 mM I^-, the k_{BPA} was increased by one to two orders of magnitude for all the four examined photocatalysts, reaching as much as 130 times for CdS (Fig. 2c). Therefore, the I^- should exhibit a widespread promoting effect in photocatalysis for degradation of pollutants, regardless of the utilization of different photocatalysts.

The pH effect for I^--mediated BPA degradation was further examined. The initial solution pH could obviously influence the BPA degradation in the KCN-I^- system (Fig. 2d), and the k_{BPA} is in the range of 1.72–4.53 h^{-1} in pH 6–9 (Table S1). Moreover, the BPA degradation efficiency is higher in neutral to weak alkaline conditions (pH 7–8) compared with stronger acidic or alkaline conditions (e.g. pH 6 and pH 9). The BPA removal efficiency is about 100% at pH 7 and pH 8, which decreased to 93% and 83% at pH 9 and pH 6, respectively. This pH-induced difference on BPA degradation efficiency could be associated with the generation of RIS, zeta potential of KCN, and the pK_a of BPA. The pH could influence the oxidation kinetic of I^- and the transformation between different kinds of RIS by involving protons as reactant [28,35]. Moreover, the zeta potential of KCN is more positive with the pH decrease (Fig. S8), suggesting more positively charged surfaces. This would favor the adsorption of electron-rich I^-, but suppress the adsorption of electron-poor O_2. Hence, the pH decrease could be a double-edged sword for RIS generation, because the direct oxidation of I^- by h^+ is favored, while the indirect oxidation of I^- by H_2O_2 generated from O_2 reduction would be suppressed. Form pH 8 to pH 9, the performance decrease of the KCN-I^- system may be also associated with the pK_a effect of BPA: with a pK_a at 9.73, the proportion of BPA molecule in the anion form would dramatically increase with pH increase from 8 to 9, which would suppress the oxidation kinetics of BPA [41].

Furthermore, the degradation of BPA in different initial concentrations were examined. As displayed in Fig. S9, when the initial concentration of BPA ($C_{0,\ BPA}$) is under 0.1 mM, the k_{BPA} remains stable between 4.53 and 5.83 h^{-1}, indicating the unaffected treatment of pollutants in lower concentration. Due to the limited amount of active species, further increase of $C_{0,\ BPA}$ to 0.2 and 0.4 mM lead to decrease of k_{BPA} to 1.38 and 0.41 h^{-1}, respectively. However, when $C_{0,\ BPA}$ increases from 0.2 to 0.4 mM, the removal amount of BPA only slightly decreases from 7.8 to 7.0 μmol, which could be further improved by adjusting the ratio of I^- and KCN. Therefore, the efficiency of the KCN-I^- system can be considered applicable for treatment of pollutants in higher or lower concentrations. With high efficiency and applicability, this I^--based photocatalytic system could offer advanced opportunities for practical treatment of organic pollutants.

3.3. Selective degradation of phenolic pollutants

The performance of the KCN-I^- system for degradation of different kinds of pollutants were examined, including phenolic pollutants (BPA, p-cresol (p-CR), 2,4-dichlorophenol (2,4-DP), 2,2′-biphenol (2,2′-BP)), pharmaceuticals (ibuprofen (IBU)), and dyes (rhodamine B (RhB)) (physicochemical properties shown in Table S2). In the presence of 40 mM I^-, the concentrations of IBU and RhB have no visible decrease (Fig. S10), indicating the seldom oxidation of these two non-phenolic pollutants in the KCN-I^- system. However, the four phenolic pollutants, are rapidly degraded, and the removal efficiencies of BPA, p-CR, and 2,4-DP, are more than 95% (Fig. 3a and S10). The degradation rate was enhanced by 8–29 times for phenolic pollutants, while the degradation of IBU and RhB are inhibited due to the presence of I^-. This result suggests the selective oxidation nature of the KCN-I^- system towards phenolic pollutants, which cannot be achieved by traditional photocatalytic processes with h^+/•OH as reactive species to oxidize organic pollutants [42,43]. The underlying mechanism should be associated with the generation of RIS with selective nature for the I^--based system [27].

Background substances commonly present in waters could remarkably inhibit the degradation of organic pollutants due to the competitive reaction with reactive species (e.g. •OH) [21–23]. Fig. 3b presents the BPA degradation on KCN in the presence of different concentrations of Cl^-. The degradation of BPA on KCN suffers from obvious hindrance in the presence of Cl^- (0.1–0.5 M), and the k_{BPA} decreases by 26–64% (Table S1). This is because •OH is the common reactive species inducing the degradation of organic pollutants in g-C_3N_4-based photocatalysis [18], and it would be readily consumed by Cl^-. However, the degradation rate of BPA for KCN-I^- system only exhibits a slight decrease (8–23%) in the presence of 0.1–0.5 M Cl^- (Table S1), while the removal efficiency remains > 99% at 60 min. Moreover, the presence of other anions (i.e. SO_4^{2-}, HCO_3^-, PO_4^-) has only moderate inhibiting effect on BPA degradation (Fig. 3c) too. The influence of organics on I^--mediated pollutant degradation is shown in Fig. 3d. These small organic molecules could act as effective scavengers of h^+/•OH [44,45], thus, significantly inhibiting the photocatalytic degradation of pollutants. Nevertheless, the presence of neither carboxylic acids nor alcohols can remarkably suppress the BPA degradation, and the k_{BPA} merely exhibits a decrease of < 8%. Moreover, it was found that the BPA degradation was only slightly suppressed by natural organic matters: the degradation rate of BPA decreased by 14% in the presence of 30 ppm humic acid (Fig. S11), which could be induced by the shading effect of humic acid. Hence, the KCN-I^- system would not suffer from significant hindrance by co-existing substances of anions and organics in water. Though interference may still be induced by other environmental background substances due to the rather complex components, the excellent selectivity of the KCN-I^- system for oxidation of phenolic pollutants could be of great significance in preventing the decrease of removal efficiency and generation of undesirable (e.g. toxic) byproducts.

3.4. Mechanism for RIS generation and pollutant degradation

The I^- could be easily oxidized in photocatalytic process by: 1) photo-induced h^+ (Eq 1) [46,47], and 2) H_2O_2 generated through e^--mediated oxygen reduction reaction (ORR, Eqs 2–3) (Table 2) [28]. The oxidation of I^- gives birth to •I, which could react rapidly with excess I^- (Eq 4) to form $•I_2^-$ at a rate constant of 8.8×10^9 M^{-1} s^{-1}. Then, rapid self-quenching of $•I_2^-$ would occur to produce I_3^- and I^- at a rate constant of 2.3×10^9 M^{-1} s^{-1} (Eq 5). Accordingly, the production of I_3^- could reflect the efficiency of •I generation from I^- oxidation.

As shown in Fig. 4a, the production of I_3^- was found in tens of μM

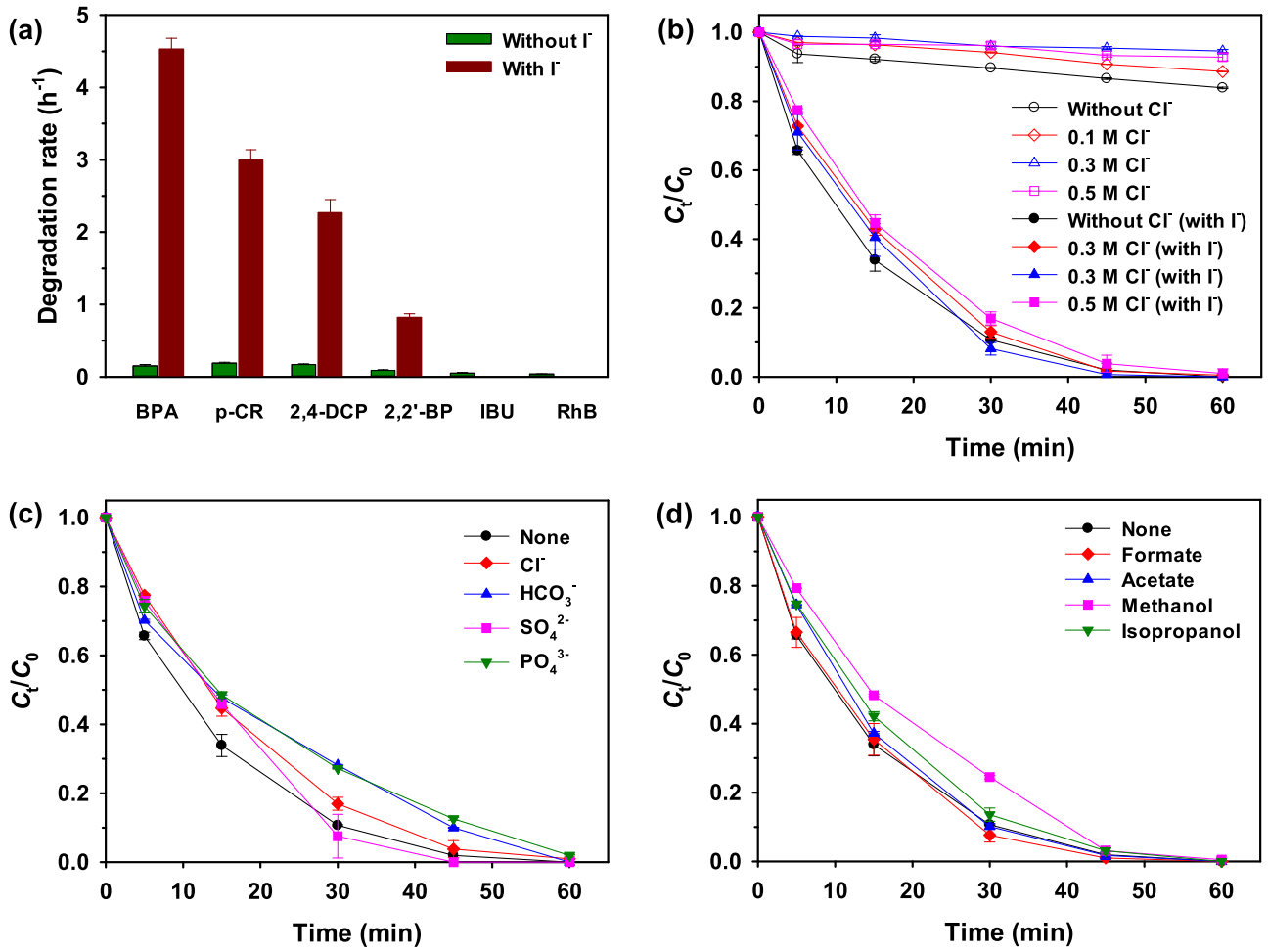

Fig. 3. (a) Photocatalytic degradation rate of different kinds of organic pollutants by the KCN-I^- system, including bisphenol A (BPA), p-cresol (p-CR), 2,2′-biphenol (2,2′-BP), and 2, 4-dichlorophenol (2,4-DP), ibuprofen (IBU) and Rhodamine B (RhB). (b) BPA degradation on KCN in the presence/absence of I^- and different concentrations of Cl^-. (c) BPA degradation by KCN-I^- system in the presence of different kinds of anions. (d) BPA degradation by KCN-I^- system in the presence of different organics. Reaction conditions: [organic pollutants]= 100 μM, [KCN]= 0.5 g/L, [I^-]= 40 mM, [anions]= 0.5 M, [organics]= 10 mM, pH 8, visible-light irradiation.

Table 2
Main reactions occurred during I–based photocatalytic system.

Equation	reaction	k (M^{-1} s^{-1})	Reference
1	$h^+ + I^- \rightarrow \bullet I$	-	-
2	$2e^- + O_2 + 2H^+ \rightarrow H_2O_2$	-	-
3	$H_2O_2 + 2I^- + 2H^+ \rightarrow 2\bullet I + 2H_2O$	4.6×10^{-4}	[35]
4	$I^- + \bullet I \rightarrow \bullet I_2^-$	8.8×10^9	[35]
5	$\bullet I_2^- + \bullet I_2^- \rightarrow I^- + I_3^-$	2.3×10^9	[35]
6	$\bullet I + \bullet I \rightarrow I_2$	1.0×10^{10}	[35]
7	$I_2 + 2H_2O \rightarrow I^- + HIO + H^+$	1.8×10^5	[50]
8	$I^- + HIO + H^+ \rightarrow I_2 + 2H_2O$	3.6×10^9	[50,51]
9	$\bullet I + Phenyl-OH \rightarrow C_6H_5O\bullet + I^- + H^+$	10^7 - 10^9	[52]
10	$\bullet I_2^- \rightarrow I^- + \bullet I$	6.9×10^4	[35]
11	$I_2 + I^- \rightarrow I_3^-$	6.2×10^9	[35]

level. The higher I_3^- yield for KCN relative to CN and Cl-CN matches well with their performance on BPA degradation (Fig. S12). To distinguish the pathway for I^- oxidation, ethanol (EtOH) was involved as a scavenger of h^+ [48], and nitro-blue tetrazolium (NBT) was used to inhibit the H_2O_2 production by quenching superoxide anion ($\bullet O_2^-$). It was found that the I_3^- production was suppressed in both cases, indicating the co-contribution of h^+ and H_2O_2 in I^- oxidation. Moreover, the more significant inhibiting effect of NBT suggests that the H_2O_2-mediated pathway is the dominant one. This result is reasonable considering the role of I^- as a h^+ sacrificial agent to boost H_2O_2 generation by improving the separation efficiency of e^--h^+ pairs. As shown in the photoluminescence (PL) spectra (Fig. S13), the PL intensity significantly decreases in the presence of I^-, indicating the inhibited recombination of e^--h^+ pairs. Besides, the effect of hole sacrificial agent for H_2O_2 generation on KCN was monitored with EtOH as an alternative to I^- [49]. The H_2O_2 yield was increased by more than 100 times in the presence of EtOH (Fig. S14). Mediated by both h^+ and e^-, the I^- oxidation in photocatalytic process could be highly efficient to rapidly produce RIS for degradation of phenolic pollutants.

The mechanism for degradation of phenolic pollutants was further investigated. The oxidants usually formed in photocatalytic process, including h^+ and •OH, have no selective nature, and could oxidize pollutants including IBU and RhB (Fig. S10) [53,54]. However, both of them were not degraded (Fig. 3a) in the KCN-I^- system. Moreover, the involvement of scavengers (EtOH for h^+, and isopropanol for •OH) only show limited inhibiting effect on BPA degradation (Fig. 5a). These results indicates that the h^+ and •OH would not directly oxidize the pollutants, because the excess I^- in the system could act as an effective

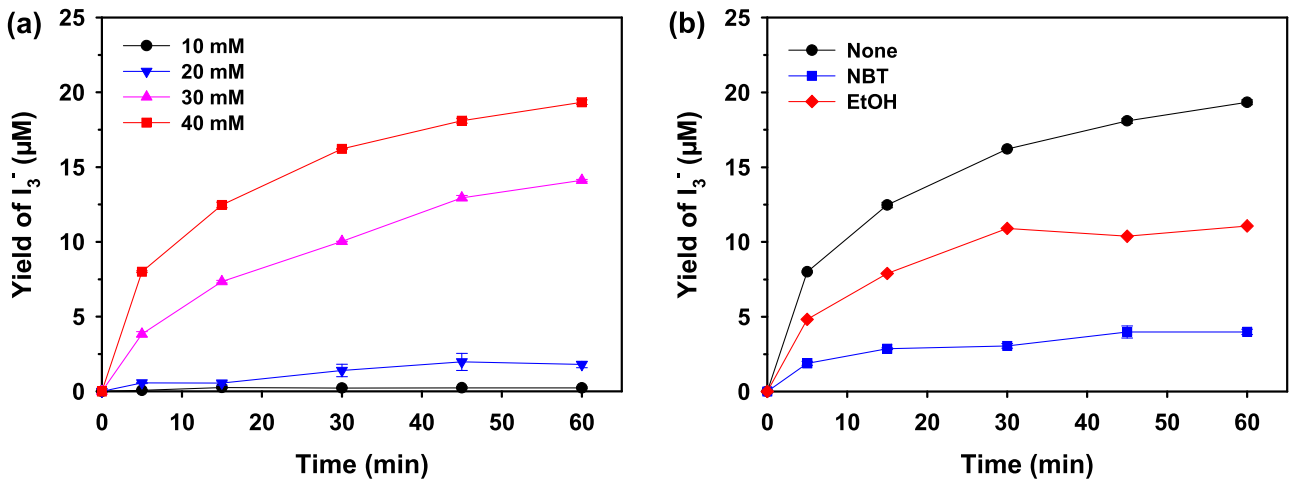

Fig. 4. (a) The generation of I_3^- on KCN with the presence of different initial concentrations of I^- under visible-light irradiation. (b) The I_3^- generation by KCN-I^- system in the presence of scavengers (NBT for $\bullet O_2^-$, and EtOH for h^+).

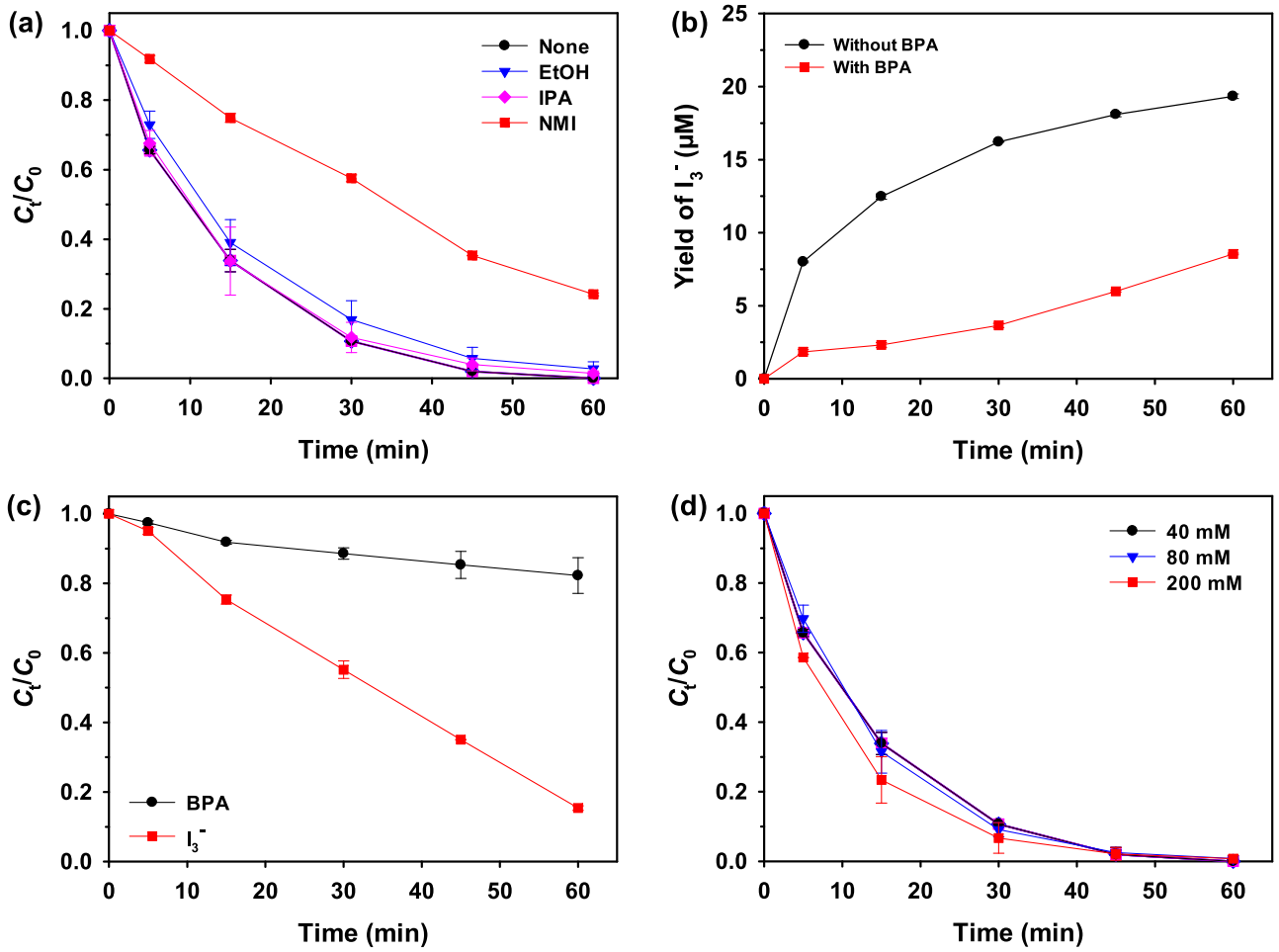

Fig. 5. (a) Degradation of BPA (100 μM) by the photocatalytic KCN-I^- system in the presence of scavengers, including 1 vol% EtOH for h^+, 100 mM isopropanol (IPA) for •OH, or 1 mM N-methylindole (NMI) for •I. (b) The production of I_3^- in the photocatalytic KCN-I^- (40 mM) system in the presence or absence of BPA (100 μM). (c) The reaction of I_3^- with BPA (100 μM) in the dark. The I_3^- was produced by the photocatalytic KCN system with I^- (40 mM) in 1 h. (d) The degradation of BPA in the presence of excess I^-.

scavenger of them [46,55].

Therefore, the RIS should be considered the dominant species for degradation of phenolic pollutants, including •I, I_3^-, •I_2^-, and HIO. As shown in Fig. 5b, the presence of BPA inhibits the generation of I_3^- in the photocatalytic KCN-I^- system, confirming the reaction between BPA and RIS. The N-methylindole (NMI) was used as an effective scavenger of •I due to the fast reaction kinetic ($k = (1.9 \pm 0.5) \times 10^{10}$ M^{-1} s^{-1}) [56]. It was found that the yield of I_3^- w inhibited completely in the presence of

1 mM NMI, suggesting the effective quenching of •I (Fig. S15). Significant inhibiting effect was observed for BPA degradation in the presence of NMI: the degradation rate was decreased by 71% (Fig. 5a). This result strongly proves the key role of RIS for BPA degradation. To show the generation of •I, the typical additive reaction with unsaturated hydrocarbon (i.e. ethylene) was performed. The production of 2-iodoethanol and ethylene glycol (Fig. S16), which should be generated from the hydrolysis of 1,2-diiodoethane [34], suggests the •I generation from I^- oxidation.

The contribution of different kinds of RIS for BPA degradation was further studied. To examine the possible oxidation of BPA by I_3^-, BPA was added to the pre-irradiated KCN-I^- system. It was found that the BPA was partially degraded, together with the decomposition of I_3^-, which confirms the I_3^--mediated BPA degradation (Fig. 5c). The steady-state concentration of I_3^- ($[I_3^-]_{ss}$) was determined to be 1.9×10^{-5} M (Fig. S17 and S18, see details in Supporting information). According to the reaction kinetic between I_3^- and BPA, the initial BPA degradation rate $k = 8.5 \times 10^{-3}$ μM s^{-1} (Fig. S19), corresponding to an initial $[I_3^-]$ at about $[I_3^-]_{ss}$ of 1.9×10^{-5} M. Hence, the I_3^--induced degradation of BPA could reaches 30.6 μM in 1-h reaction, 30.6% of the initial concentration of BPA (100 μM). Besides, HIO is another potential RIS generated during I^- oxidation process (Eqs 6–7). However, in the presence of excess I^-, the HIO tends to rapidly react with I^- to form I_2 at a rate of 3.6×10^9 M^{-1} s^{-1} (Eq 8) [50], while the rate constant for I_2 to HIO is merely 1.8×10^5 M^{-1} s^{-1}. The calculated IO^- yield according to the equilibrium constant for reversible reaction (Eqs 7–8) is much lower relative to I_2 and I_3^-, merely 1.4 μM after 1-h irradiation (Fig. S20). Therefore, the IO^--induced degradation of BPA (initially at 100 μM) can be considered negligible.

The •I is the primary oxidation product of I^-, which could react rapidly with the electron-rich groups in compounds via one-electron transfer (Eq 9), such as the phenolic hydroxyl groups in 4-methoxyphenol ($(5.7 \pm 1.2) \times 10^9$ M^{-1} s^{-1}) [31,52]. Excess I^- could inhibit the •I-mediated oxidation process by promoting the formation of $•I_2^-$ (Eq 4, $k = 8.8 \times 10^9$ M^{-1} s^{-1}) [57]. The BPA degradation in the presence of high-concentration I^- was further examined, and no obvious inhibiting effect was observed even when the concentration of I^- was increased to 200 mM (Fig. 5d). This result suggests the key role of $•I_2^-$ for BPA degradation. To compare the relative importance of •I to $•I_2^-$, their production can be estimated by the equilibrium constant of the reversible reaction (Eq 4 and 10). The concentration of $•I_2^-$ was calculated to be 5.2×10^3 times of •I. The $[•I]_{ss}$ and $[•I_2^-]_{ss}$ was determined to be 4.4×10^{-10} and 2.3×10^{-6} M, respectively. Moreover, the reaction rate of •I with I^- (8.5×10^9 M^{-1} s^{-1}) is also faster than that with phenolic pollutants (e.g. $(7.5 \pm 2.4) \times 10^7$ M^{-1} s^{-1} for p-cresol, $(1.6 \pm 0.6) \times 10^7$ M^{-1} s^{-1} for phenol) [56]. Given the excess I^- in our system (40 mM), the role of •I on phenolic pollutant (0.1 mM) degradation could be negligible. These results strongly evidence key role of $•I_2^-$ for BPA degradation, whose contribution could reach 69.4% (the other 30.6% for I_3^-).

More insights were obtained into the pH-dependent performance of the KCN-I^- system on BPA degradation. The generation of RIS in different pH was shown in Fig. S22, the I_2 and I_3^- generation are enhanced with the pH decrease, while the generated IO^- is negligible in all tested pH. This phenomenon can be ascribed to the favorable I^- oxidation in acidic conditions [58]. When the pH decreases from 8 to 6, due to the efficient •I generation from I^- oxidation, the sufficient •I tend to combine together to form I_2 (Eq 6, $k = 1.0 \times 10^{10}$ $M^{-1}{\cdot}s^{-1}$) and subsequently I_3^- (Eq 11) as revealed in Fig. S22 [35]. Accordingly, the combination of •I with I^- to form $•I_2^-$ in a lower rate ($k = 8.8 \times 10^9$ $M^{-1}{\cdot}s^{-1}$) should be inhibited, thus, leading to fewer production of $•I_2^-$ for BPA degradation. Moreover, when the pH is higher (i.e. pH 9), the generation of RIS is remarkably suppressed due to the unfavourable I^- oxidation. Therefore, the efficiency for I^--based photocatalytic degradation is pH-dependent, though it can be still considered a high-efficiency process in common weak acidic and alkaline waters.

Based on above discussion, the photocatalytic RIS generation for degradation of phenolic pollutants can be summarized as Fig. 6. Briefly,

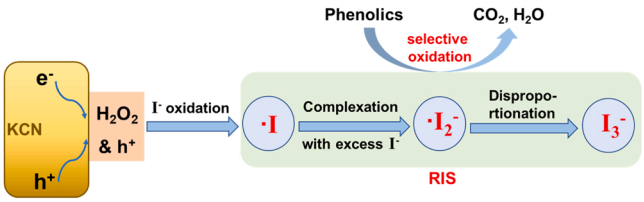

Fig. 6. Schematic illustration of RIS generation in photocatalytic process and the degradation of phenolic pollutants.

the photocatalyst can be excited to generate h^+ and e^- under irradiation, which are able to mediate I^- oxidation by direct oxidation or indirect oxidation by H_2O_2 derived from O_2 reduction reaction. Due to presence of excess I^-, the evolved •I tends to exist in the form of $•I_2^-$ derived from the complexation with I^-. Finally, the $•I_2^-$ may also transfers into I_3^- via disproportionation. All the three kinds of RIS could degrade phenolics, while the $•I_2^-$ serves as the dominant oxidant in our system. Notably, the RIS would transfer into I^- after reactions.

3.5. Cyclic utilization of the KCN-I^- system

Besides the high efficiency for degradation of phenolic pollutants, the KCN-I^- system could be a favorable system for cyclic utilization in terms of: (1) the good stability of g-C_3N_4-based photcatalyst, (2) the cyclic transformation between I^- and RIS. To examine this hypothesis, cycling experiments were conducted. After each cycle, BPA was added to reach the initial concentration (100 μM), and the KCN-I^- system was then directly subject to irradiation. As shown in Fig. 7, the degradation efficiency of BPA in the 5th cycle is 95.4%, which is close to that in the first cycle (99.1%). Therefore, the KCN-I^- system can fulfill cyclic utilization for degradation of phenolic pollutants without supply of additional chemicals. The cycling of I^-/RIS should be associated with the simultaneous generation of oxidizing h^+ and reducing e^-, which could maintain the balance between I^- and RIS. For example, the reductive decomposition of I_3^- was found to be enhanced in the presence of KCN (Fig. S23). Moreover, the KCN before and after I^--involved photoreaction is characterized by FT-IR, and no visible difference was found, which indicates the good stability of KCN (Fig. S24).

3.6. Evaluation of degradation intermediates

As displayed in Fig. S10, three of the phenolic pollutants (100 μM) suffer from almost complete degradation (> 95%) by the photocatalytic KCN-I^- (40 mM) system within 1 h. To investigate the degradation mechanism of phenolic pollutants, LC-MS analysis was carried out with

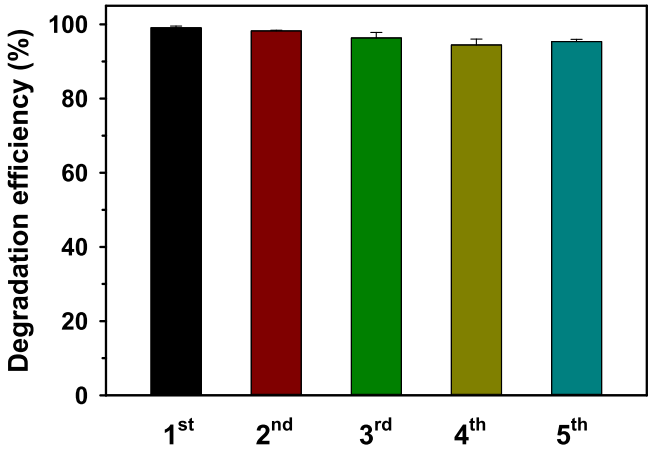

Fig. 7. Cyclic photocatalytic degradation of BPA using the KCN-I^- system by circulative adding BPA to the initial concentration (100 μM).

p-cresol as the target pollutant due to its simple molecular structure. Several peaks were identified as the generated intermediates, including $[M-H]^-$ at 107 (P1), 157 (P2), 186 (P3), 97 (P4), and 361 (P5) (Fig. S25). Moreover, the partial mineralization was revealed by the total organic carbon (TOC) measurements (Fig. S26). Accordingly, the possible degradation pathway of p-cresol was then proposed and shown in Fig. S27. The initial oxidation of p-cresol to P2 due to the transformation of phenolic -OH group suggests the typical oxidation of phenolic compounds by RIS in the KCN-I^- system.

To evaluate the production of iodinated intermediates, the total organic iodine (TOI) content during p-cresol degradation was determined according to previous reports [59,60]. The TOI gradually increase during the degradation of p-cresol by KCN-I^- photocatalytic system, suggesting the generation of iodinated organic compounds (Fig. S28). However, the highest TOI content occurs at 2.3 μM, merely 2.3% of the initial concentration of p-cresol. Moreover, a slight decrease of TOI occurs from 45 min to 60 min, which indicates that TOI may further decrease during long-term photoreaction. As the LC_{50} of the potential by-products are mainly ranging from 0.1 to 1 mM [61], the generation of TOI in several μM is less likely to cause environmental concerns. Even so, future works for optimizing the KCN-I^- system to minimize the generation of iodinated compounds should be certainly beneficial.

4. Conclusion

Efficient and selective removal of phenolic pollutants in water by green and sustainable approaches is of great significance for environmental treatment. Here we found that the I^--based photocatalytic process is a promising strategy for this purpose. Being thermodynamically favorable to be oxidized, I^- can be efficiently converted to RIS including $\bullet I$, $\bullet I_2$, and I_3^- by both h^+- and e^--mediated processes. Taking advantage of the nature of RIS, selective oxidation of phenolic pollutants becomes possible. As the oxidants are not consumed by the matrix species, this approach is less likely to generate toxic byproducts. Given the successful cycling of I^- and RIS, a practical solar-driven photocatalytic I^- system can be set up for the degradation of phenolics without further input of energy and chemicals.

CRediT authorship contribution statement

Liangpang Xu: Methodology, Conceptualization, Software, Investigation, Resources, Data curation, Writing – original draft. **Po Keung Wong**: Formal analysis, Writing – review & editing. **Zhifeng Jiang**: Conceptualization, Methodology, Writing – review & editing, Funding acquisition. **Jimmy C. Yu:** Conceptualization, Writing – review & editing, Supervision, Funding acquisition.

Declaration of Competing Interest

We declare that we have no known competing financial interests or personal relationships that could have appeared to influence the work reported in this paper.

Data Availability

Data will be made available on request.

Acknowledgement

This work was supported by the Research Grants Council of Hong Kong (Project 14304019), National Natural Science Foundation of China (Grant No. 22178149), Natural Science Foundation of Jiangsu Province for Outstanding Youth Scientists (BK20211599), and Key Research and Development Project of Zhenjiang City (CQ2022001).

Appendix A. Supporting information

Supplementary data associated with this article can be found in the online version at doi:10.1016/j.apcatb.2023.123080.

References

[1] J. Michałowicz, W. Duda, Phenols–sources and toxicity, Pol. J. Environ. Stud. 16 (2007).
[2] G. Busca, S. Berardinelli, C. Resini, L. Arrighi, Technologies for the removal of phenol from fluid streams: a short review of recent developments, J. Hazard. Mater. 160 (2008) 265–288.
[3] S. Hosseini, S. Borghei, M. Vossoughi, N. Taghavinia, Immobilization of TiO_2 on perlite granules for photocatalytic degradation of phenol, Appl. Catal. B 74 (2007) 53–62.
[4] J. Lee, U. Von Gunten, J.-H. Kim, Persulfate-based advanced oxidation: critical assessment of opportunities and roadblocks, Environ. Sci. Technol. 54 (2020) 3064–3081.
[5] L. Zhou, W. Song, Z. Chen, G. Yin, Degradation of organic pollutants in wastewater by bicarbonate-activated hydrogen peroxide with a supported cobalt catalyst, Environ. Sci. Technol. 47 (2013) 3833–3839.
[6] T. Al-Khalid, M.H. El-Naas, Aerobic biodegradation of phenols: a comprehensive review, Crit. Rev. Environ. Sci. Technol. 42 (2012) 1631–1690.
[7] S.K. Loeb, P.J. Alvarez, J.A. Brame, E.L. Cates, W. Choi, J. Crittenden, D. D. Dionysiou, Q. Li, G. Li-Puma, X. Quan, The technology horizon for photocatalytic water treatment: sunrise or sunset? Environ. Sci. Technol. 53 (2019) 2937–2947.
[8] F. He, Z. Wang, Y. Li, S. Peng, B. Liu, The nonmetal modulation of composition and morphology of g-C_3N_4-based photocatalysts, Appl. Catal. B 269 (2020), 118828.
[9] X. Li, J. Xie, C. Jiang, J. Yu, P. Zhang, Review on design and evaluation of environmental photocatalysts, Front. Environ. Sci. Eng. 12 (2018) 1–32.
[10] M. Zhou, H. Ou, S. Li, X. Qin, Y. Fang, Sc Lee, X. Wang, W. Ho, Photocatalytic air purification using functional polymeric carbon nitrides, Adv. Sci. 8 (2021) 2102376.
[11] H. Park, Y. Park, W. Kim, W. Choi, Surface modification of TiO2 photocatalyst for environmental applications, J. Photochem. Photobiol. C: Photochem. Rev. 15 (2013) 1–20.
[12] H. Dong, G. Zeng, L. Tang, C. Fan, C. Zhang, X. He, Y. He, An overview on limitations of TiO_2-based particles for photocatalytic degradation of organic pollutants and the corresponding countermeasures, Water Res. 79 (2015) 128–146.
[13] H. Wang, L. Zhang, Z. Chen, J. Hu, S. Li, Z. Wang, J. Liu, X. Wang, Semiconductor heterojunction photocatalysts: design, construction, and photocatalytic performances, Chem. Soc. Rev. 43 (2014) 5234–5244.
[14] L. Zhang, J. Zhang, H. Yu, J. Yu, Emerging S-scheme photocatalyst, Adv. Mater. 34 (2022) 2107668.
[15] H. Li, J. Shang, H. Zhu, Z. Yang, Z. Ai, L. Zhang, Oxygen vacancy structure associated photocatalytic water oxidation of BiOCl, ACS Catal. 6 (2016) 8276–8285.
[16] L. Xu, L. Li, Z. Hu, J.C. Yu, Boosting alkaline photocatalytic H_2O_2 generation by incorporating pyrophosphate on g-C_3N_4 for effective proton shuttle and oxygen activation, Appl. Catal. B (2023), 122490.
[17] L. Xu, L. Li, L. Yu, J.C. Yu, Efficient generation of singlet oxygen on modified g-C_3N_4 photocatalyst for preferential oxidation of targeted organic pollutants, Chem. Eng. J. 431 (2022), 134241.
[18] J. Lim, H. Kim, J. Park, G.-H. Moon, J.J.M. Vequizo, A. Yamakata, J. Lee, W. Choi, How g-C_3N_4 works and is different from TiO_2 as an environmental photocatalyst: mechanistic view, Environ. Sci. Technol. 54 (2019) 497–506.
[19] W.R. Haag, C.D. Yao, Rate constants for reaction of hydroxyl radicals with several drinking water contaminants, Environ. Sci. Technol. 26 (1992) 1005–1013.
[20] F. Chen, L.-L. Liu, J.-J. Chen, W.-W. Li, Y.-P. Chen, Y.-J. Zhang, J.-H. Wu, S.-C. Mei, Q. Yang, H.-Q. Yu, Efficient decontamination of organic pollutants under high salinity conditions by a nonradical peroxymonosulfate activation system, Water Res. 191 (2021), 116799.
[21] C.-H. Liao, S.-F. Kang, F.-A. Wu, Hydroxyl radical scavenging role of chloride and bicarbonate ions in the H_2O_2/UV process, Chemosphere 44 (2001) 1193–1200.
[22] J. Brame, M. Long, Q. Li, P. Alvarez, Trading oxidation power for efficiency: differential inhibition of photo-generated hydroxyl radicals versus singlet oxygen, Water Res. 60 (2014) 259–266.
[23] D.D. Phong, J. Hur, Insight into photocatalytic degradation of dissolved organic matter in UVA/TiO_2 systems revealed by fluorescence EEM-PARAFAC, Water Res. 87 (2015) 119–126.
[24] Y. Kamaya, Y. Fukaya, K. Suzuki, Acute toxicity of benzoic acids to the crustacean Daphnia magna, Chemosphere 59 (2005) 255–261.
[25] P.R. Harvey, R. Rudham, Photocatalytic oxidation of iodide ions by titanium dioxide, J. Chem. Soc., Faraday Trans. 1 (84) (1988) 4181–4190.
[26] J.E. Grebel, J.J. Pignatello, W.A. Mitch, Effect of halide ions and carbonates on organic contaminant degradation by hydroxyl radical-based advanced oxidation processes in saline waters, Environ. Sci. Technol. 44 (2010) 6822–6828.
[27] Y. Feng, P.-H. Lee, D. Wu, K. Shih, Rapid selective circumneutral degradation of phenolic pollutants using peroxymonosulfate–iodide metal-free oxidation: role of iodine atoms, Environ. Sci. Technol. 51 (2017) 2312–2320.
[28] Z. Chen, J. Li, K.Y. Koh, Z. Du, C.N. Ong, J.P. Chen, Kinetics and mechanism investigation of selective arsenite oxidation by reactive iodine species in hydrogen peroxide and iodide (H_2O_2/I^-) system, ACS ES&T Water 1 (2021) 1515–1523.

[29] H. Hou, X. Zeng, X. Zhang, Production of hydrogen peroxide by photocatalytic processes, Angew. Chem. Int. Ed. 59 (2020) 17356–17376.
[30] D.M. Stanbury, Reduction potentials involving inorganic free radicals in aqueous solution. Adv. Inorg. Chem, Elsevier,, 1989, pp. 69–138.
[31] P. Neta, R.E. Huie, A.B. Ross, Rate constants for reactions of inorganic radicals in aqueous solution, J. Phys. Chem. Ref. Data 17 (1988) 1027–1284.
[32] M.E. Langmuir, E. Hayon, Flash photolysis study of mercury (II) halide complexes in aqueous solutions. Rates of reaction X2-radical anions, J. Phys. Chem. A 71 (1967) 3808–3814.
[33] J.G. Rowley, B.H. Farnum, S. Ardo, G.J. Meyer, Iodide chemistry in dye-sensitized solar cells: making and breaking I-I bonds for solar energy conversion, J. Phys. Chem. Lett. 1 (2010) 3132–3140.
[34] L. Xu, Y. Xie, L. Li, Z. Hu, Y. Wang, 57, Highly selective photocatalytic synthesis of ethylene-derived commodity chemicals on BiOBr nanosheets, Mater. Today Phys. 21 (2021), 100551.
[35] M.C. Milenkovic, D.R. Stanisavljev, Role of free radicals in modeling the iodide-peroxide reaction mechanism, J. Phys. Chem. A 116 (2012) 5541–5548.
[36] T. Xiong, W. Cen, Y. Zhang, F. Dong, Bridging the g-C_3N_4 interlayers for enhanced photocatalysis, ACS Catal. 6 (2016) 2462–2472.
[37] X. Sun, D. Jiang, L. Zhang, W. Wang, Alkaline modified g-C_3N_4 photocatalyst for high selective oxide coupling of benzyl alcohol to benzoin, Appl. Catal. B 220 (2018) 553–560.
[38] W.-J. Ong, L.-L. Tan, Y.H. Ng, S.-T. Yong, S.-P. Chai, Graphitic carbon nitride (g-C_3N_4)-based photocatalysts for artificial photosynthesis and environmental remediation: are we a step closer to achieving sustainability? Chem. Rev. 116 (2016) 7159–7329.
[39] M. Xiao, B. Luo, S. Wang, L. Wang, Solar energy conversion on g-C_3N_4 photocatalyst: light harvesting, charge separation, and surface kinetics, J. Energy Chem. 27 (2018) 1111–1123.
[40] B. Reichman, C.E. Byvik, Photoproduction of I_2, Br_2, and Cl_2 on n-semiconducting powder, J. Phys. Chem. 85 (1981) 2255–2258.
[41] Y. Ding, P. Zhou, H. Tang, Visible-light photocatalytic degradation of bisphenol A on $NaBiO_3$ nanosheets in a wide pH range: a synergistic effect between photocatalytic oxidation and chemical oxidation, Chem. Eng. J. 291 (2016) 149–160.
[42] A. Kumar, M. Khan, J. He, I.M. Lo, Visible-light-driven magnetically recyclable terephthalic acid functionalized g-C_3N_4/TiO_2 heterojunction nanophotocatalyst for enhanced degradation of PPCPs, Appl. Catal. B 270 (2020), 118898.
[43] X. Liu, Y. Du, Y. Zhao, X. Song, X. Jing, L. Yu, M. Sun, 2D Benzodithiophene based conjugated polymer/g-C_3N_4 heterostructures with enhanced photocatalytic activity: Synergistic effect of antibacterial carbazole side chain and main chain copolymerization, Appl. Catal. B 312 (2022), 121401.
[44] C.-Y. Chu, M.H. Huang, Facet-dependent photocatalytic properties of Cu2O crystals probed by using electron, hole and radical scavengers, J. Mater. Chem. A 5 (2017) 15116–15123.
[45] T. Tan, D. Beydoun, R. Amal, Effects of organic hole scavengers on the photocatalytic reduction of selenium anions, J. Photochem. Photobiol. A 159 (2003) 273–280.
[46] N. Gupta, B. Pal, Photocatalytic activity of transition metal and metal ions impregnated TiO2 nanostructures for iodide oxidation to iodine formation, J. Mol. Catal. A 371 (2013) 48–55.
[47] C. Karunakaran, P. Anilkumar, Semiconductor-catalyzed solar photooxidation of iodide ion, J. Mol. Catal. A 265 (2007) 153–158.
[48] D. Gao, J. Xu, F. Chen, P. Wang, H. Yu, Unsaturated selenium-enriched $MoSe_{2+x}$ amorphous nanoclusters: One-step photoinduced co-reduction route and its boosted photocatalytic H_2-evolution activity for TiO_2, Appl. Catal. B 305 (2022), 121053.
[49] Y. Yang, B. Zhu, L. Wang, B. Cheng, L. Zhang, J. Yu, In-situ grown N, S co-doped graphene on TiO_2 fiber for artificial photosynthesis of H_2O_2 and mechanism study, Appl. Catal. B 317 (2022), 121788.
[50] S. Furrow, Reactions of iodine intermediates in iodate-hydrogen peroxide oscillators, J. Phys. Chem. A 91 (1987) 2129–2135.
[51] G. Schmitz, Iodine oxidation by hydrogen peroxide in acidic solutions, Bray-Liebhafsky reaction and other related reactions, Phys. Chem. Chem. Phys. 12 (2010) 6605–6615.
[52] Z. Alfassi, R. Huie, S. Marguet, E. Natarajan, P. Neta, Rate constants for reactions of iodine atoms in solution, Int. J. Chem. Kinet. 27 (1995) 181–188.
[53] S. Yan, Z. Li, Z. Zou, Photodegradation of rhodamine B and methyl orange over boron-doped g-C_3N_4 under visible light irradiation, Langmuir 26 (2010) 3894–3901.
[54] J. Wang, L. Tang, G. Zeng, Y. Deng, Y. Liu, L. Wang, Y. Zhou, Z. Guo, J. Wang, C. Zhang, Atomic scale g-C_3N_4/Bi_2WO_6 2D/2D heterojunction with enhanced photocatalytic degradation of ibuprofen under visible light irradiation, Appl. Catal. B 209 (2017) 285–294.
[55] J. Thomas, Rates of reaction of the hydroxyl radical, Trans. Faraday Soc. 61 (1965) 702–707.
[56] Z. Alfassi, R. Huie, S. Marguet, E. Natarajan, P. Neta, Rate constants for reactions of iodine atoms in solution, Int. J. Chem. Kinet. 27 (1995) 181–188.
[57] A.J. Elliot, A pulse radiolysis study of the reaction of OH with I_2 and the decay of I_2^-, Can. J. Chem. 70 (1992) 1658–1661.
[58] J.-M. Herrmann, P. Pichat, Heterogeneous photocatalysis. Oxidation of halide ions by oxygen in ultraviolet irradiated aqueous suspension of titanium dioxide, J. Chem. Soc. Faraday Trans. 1 (76) (1980) 1138–1146.
[59] Y. Pan, X. Zhang, Total organic iodine measurement: a new approach with UPLC/ESI-MS for off-line iodide separation/detection, Water Res. 47 (2013) 163–172.
[60] B. Chen, Y. Bu, J. Yang, W. Nian, S. Hao, Methods for total organic halogen (TOX) analysis in water: past, Present Future Chem. Eng. J. 399 (2020), 125675.
[61] H. Dong, Z. Qiang, S.D. Richardson, Formation of iodinated disinfection byproducts (I-DBPs) in drinking water: emerging concerns and current issues, Acc. Chem. Res. 52 (2019) 896–905.